Cement and Concrete Research 40 (2010) 33–44

Contents lists available at ScienceDirect

Cement and Concrete Research

journal homepage: http://ees.elsevier.com/CEMCON/default.asp

An investigation of microstructure evolution in cement paste through setting using ultrasonic and rheological measurements

Kolluru V. Subramaniam *, Xiaojun Wang

Civil Engineering Department, City College of the City University of New York, New York, NY 10031, United States

ARTICLE INFO

Article history:
Received 22 October 2008
Accepted 24 September 2009

Keywords:
Microstructure (B)
Porosity (B)
Rheology (C)
Ultrasonic Testing (B)
Setting (C)

ABSTRACT

The response of hydrating cement paste through setting are monitored using rheological measurements and ultrasonic reflection measurements. Increases in the elastic modulus and yield stress of cement paste with time are obtained from the rheological measurements. Ultrasonic measurements are performed using horizontally polarized shear waves (SH) reflected off of the hydrating cement paste. Changes in the ultrasonic signal through setting are related with changes in the porosity and stiffness of an equivalent water-filled poroelastic material, which provides identical acoustic impedance. The measured changes in the shear modulus obtained from ultrasonic measurement are shown to correlate well with increase in elastic modulus obtained from rheological measurements. The increase in the shear modulus of the porous material obtained from the ultrasonic measurements is shown to correspond well with the observed increase in the yield stress of the cement paste. By combining the information from rheological and ultrasonic measurements, it is found that even in the fluid stage there is sufficient structural integrity in the arrangement of cement grains to support low-amplitude shear stress and the evolution of a continuously connected network of cement particles within the paste is coincident with a rapid increase in the shear modulus of the porous skeleton.

© 2009 Elsevier Ltd. All rights reserved.

1. Introduction

Accurate determination of the changes in the microstructure through setting, which result in an increased capacity of the hydrating cement paste to resist applied shear stress has remained a major experimental challenge. Conventional methods for probing the microstructure are not conducive to studying changes in microstructure in the first few hours after casting since sample preparation procedures either alter or disturb the microstructure and the changes in microstructure occur on a time scale that is an order of magnitude faster than the time required for sample preparation [1]. Limited studies on direct observation of evolution of the solid phase from within the fluid medium and changes in the microstructure of hardening solid phase of the cementitious material using X-ray techniques [2,3] and small angle neutron scattering (SANS) [4] have been reported recently. These methods, which provide information about the evolution of microstructure in cement paste however, do not simultaneously provide information about the mechanical properties of the material. Mechanical and vibration-based techniques which provide reliable measures of elastic material properties on the other hand do not provide information about the microstructure and are not applicable during setting. In the absence of a direct measurement of microstructural variables the current understanding of the microstructure changes during setting of cement pastes has been developed by application of computer-based models which simulate the development of microstructure [5,6].

Setting behavior is usually investigated using penetration tests (vicat or pin penetration), which provide a measure of resistance to penetration. The approximate time for the emergence of a solid skeleton is identified from the resistance to penetration of an indenter. Such a measurement does not allow for evaluating the properties of the solid skeleton since no data pertaining to deformation of the material is collected. Immediately following the emergence of a connected network of hydration products from within the fluid medium, the resulting solid is very weak and obtaining reliable values from penetration measurements is not possible due to limitations of force detecting capabilities. Probing cement paste using ultrasonic waves provides reliable low stress measurement, which does not perturb the microstructure. Ultrasonic waves have been shown to sensitively monitor the buildup of structure inside the cement paste [7–10]. Ultrasonic wave propagation through a material depends upon its elastic mechanical properties, which in turn can be related to its microstructure [7,8].

In typical ultrasonic measurements, compression (P) or shear (S) waves are used in arrangements which are based on transmission through the material or on reflection at the interface of the cementitious material. The different ultrasonic techniques used for

* Corresponding author. Tel.: +1 212 650 6569; fax: +1 212 650 6965.
E-mail address: ksubram@ce.ccny.cuny.edu (K.V. Subramaniam).

0008-8846/$ – see front matter © 2009 Elsevier Ltd. All rights reserved.
doi:10.1016/j.cemconres.2009.09.018

cementitious materials are reviewed in Ref. [11]. Since cementitious materials are initially in a liquid state, and liquids have very low shear modulus, the through transmission techniques using S waves do not provide reliable results in this stage. Through transmission measurements are influenced by the attenuation of medium, which can significantly influence the early age measurements. Also, the constraints on the specimen size imposed by the high attenuation of the cementitious materials in the early ages accentuates the influence of the interface effect since there are two interfaces in a through transmission measurement. Reflection measurements using shear waves are particularly suited for measurements in the early ages, during setting, and have been shown to be very sensitive to changes in state since there is a large change in shear modulus associated with the fluid–solid transformation [12].

The primary focus of the research presented here is to assess changes in the microstructure of a hydrating cement paste through the early stages of hydration and the setting process. Two different measurements were concurrently performed on cement paste samples after mixing. The rheological response of cement paste was examined up to the initiation of setting using low amplitude oscillatory shear and yield stress measurements. Changes in an ultrasonic shear wave produced by a reflection off of the hydrating cement paste were also monitored. Such measurements have previously been used for studying the evolution of strength and visco-elastic properties of hydrating cementitious materials [9,12–15]. More elaborate experimental test setup than used previously is presented. The theoretical framework necessary to interpret the results of the ultrasonic technique and provide information about the microstructure of the hydrating cement paste in terms of physically-based variables is developed using the poroelastic theory. Poroelastic theory has been used for studying porous media such as rocks, and soils [16–21] and offers a natural way for modeling the hydrating cement system [8]. An understanding of the microstructure evolution through setting is obtained by combining the information obtained from the ultrasonic measurements with the observed changes in the rheological behavior.

2. Background

Setting and increase in elastic stiffness in a hydrating cement paste is a very complex multi-scale phenomenon involving changes in state and the internal structure, with time [22,23]. The change in state can be visualized as a transformation of cement paste from a material in which bulk flow is produced at relatively low applied shear stress, to a solid where significantly high stress is required to produce small strain. The fluid state may be characterized as a suspension of cement grains in water with an internal structure comprised of arrangements of grains. At large strains, there is a reorganization of the internal structure which results in a different arrangement of grains. There is no change in the nominal values of bulk material properties due to this rearrangement of internal structure in the fluid state. The solid state is characterized by the existence of a long-range order in the microstructure due to the presence of bonds between the individual cement grains. In a solid, irreversible changes associated with complete disruption of the microstructure, resulting from breaking of bonds, are produced at large strains.

Our current understanding of changes in the microstructure during setting obtained from the computer simulation models [5,6] indicates that initially, a weak skeleton emerges from within the fluid medium when the products of hydration link up to provide a continuous network of solid within the fluid-filled space. The emergence of a continuous solid phase within the fluid medium has been identified as the percolation threshold [5,6]. Following percolation threshold, setting behavior is initiated in the cement paste. Through setting, as the products of hydration form within the fluid-filled spaces of cement paste, a network of pores and a pore structure develop.

2.1. Idealization of the cement paste

The poroelastic framework proposed by Biot provides realistic representation of for developing constitutive relations for hydrating cement paste [24–26]. According to Biot's theory, the volume fraction of the fluid within a unit volume of the material is referred to as the porosity. It is implicitly assumed that the walls of the pores are impervious and the pore size is concentrated around its average value. The pore structure is assumed to be comprised of inter-connected void space, which allows motion of the fluid relative to the solid. The porous solid and the solid–fluid system are assumed to be statistically isotropic. The propagation of waves in the fluid-saturated poroelastic medium depends upon the internal system variables such as, the effective elastic properties of the porous solid, the porosity, and the parameters related to the pore structure, which influence the flow of the fluid in the porous solid.

Considering a fluid-saturated porous solid, a pair of coupled displacement equations of motion governing both rotational and dilatational motions is obtained by combining the Biot's constitutive relationship and Darcy's law for flow through a porous medium [26]

$$\mu_b\nabla^2\vec{u}+(H-2\mu_b)\nabla(\nabla\cdot\vec{u})-C\nabla(\nabla\cdot\vec{w})=\rho\ddot{\vec{u}}-\rho_f\ddot{\vec{w}} \tag{1a}$$

$$C\nabla(\nabla\cdot\vec{u})-M\nabla(\nabla\cdot\vec{w})=\rho_f\ddot{\vec{u}}-m'\ddot{\vec{w}}-{}^{\eta}/_{\kappa}\dot{w} \tag{1b}$$

where the average displacement of solid skeletal frame and the fluid are denoted by $\vec{u}=\vec{u}(x,t)$ and $\vec{U}=\vec{U}(x,t)$, respectively, $\vec{w}(x,t)=\beta(\vec{u}-\vec{U})$ is the relative displacement of fluid and skeletal frame, β is the void volume fraction of the fluid or porosity (assumed to be isotropic), $\rho=(1-\beta)\rho_s+\beta\rho_f$ is the total mass density, ρ_s is the solid mass density, ρ_f is fluid mass density, η is the fluid viscosity, and κ is the coefficient of permeability of the porous frame, $m'=c\rho_f/\beta$, c is the tortuosity coefficient (dimensionless parameter), which is a experimentally determined, μ_b is the shear modulus of the skeletal frame (under drained conditions). In Equation(s) (1), H,C and M represent operators that characterize the response of the composite, and are given as [18]

$$H=\frac{(K_s-K_b)^2}{D-K_b}+K_b+\frac{4\mu_b}{3} \tag{2a}$$

$$M=\frac{K_s^2}{D-K_b} \tag{2b}$$

$$C=\frac{K_s(K_s-K_b)}{D-K_b} \tag{2c}$$

where K_b is the bulk modulus of the skeletal frame (under drained conditions), $D=K_s(1+\beta\frac{K_s}{K_f-1})$, K_s is the bulk modulus of the material of the skeletal frame and K_f is the bulk modulus of the pore fluid. The solutions of Equation(s) (1) for a specific set of boundary and initial conditions yield expressions for displacements and stresses in a poroelastic medium due to wave propagation. Solutions for these equations have been worked out by several researchers [16,27].

In order to employ Biot's porous model, thirteen material constants are required, and independent experimental measurements would be necessary to obtain these parameters. However, as presented by Berryman [28], the analysis can be simplified considering inter-relations between some of the material parameters. In Berryman's approach, the tortuosity of porous media is estimated theoretically and is given as

$$c=1-r(1-1/\beta). \tag{3}$$

In general, the value of r must be calculated from a microscopic model of the frame moving in the fluid. It was found that the value of r equal to ½, which is the exact value for the case of spheres in a fluid medium provided a reasonable estimate for a porous medium with

constant porosity within the range $\beta < 0.4$. The relationship between permeability, pore size and porosity, can be obtained from the Kozeny–Carman relation and is given as

$$\kappa(1-\beta)^2/\beta^3 = \kappa_0(1-\beta_0)^2/\beta_0^3 = const. \quad (4a)$$

and similarly

$$a^2/\kappa = a_0^2/\kappa_0 = const. \quad (4b)$$

where α is the pore diameter.

The predicted wave propagation using Berryman's simplifications was comparable to the experimental results obtained by Plona [29], on fine grained sands and sintered porous glass. It was shown that the assumptions in Eqs. (3) and (4), provide a reliable way for evaluating parameters, which leads to an accurate description of elastic wave propagation in fluid-saturated porous media. The results were also found to be insensitive to the exact relationships between porosity of the solid and properties which influence flow of the fluid such as permeability and tortuosity. From their experiments on model systems considering glass beads, it was shown that the differences between the response of a free arrangement of glass beads and fused beads could clearly be identified using ultrasonic waves. In the free arrangement of glass beads there was no bonding between the individual beads. The fused system was obtained by applying pressure and heat to the free arrangement resulting in a structure where the glass beads were fused at the points of contact. While there was a negligible difference in the porosity, there was a considerable difference in the elastic stiffness of the porous solid for the two systems [16].

3. Experimental test program

Cement paste samples were mixed using a paddle mixer following a procedure suggested by Williams et al. [30], which is similar to the procedure given in ASTM C-305 [31]. Cement and water were initially mixed at 140 rpm for 30 s, followed by a pause for 1 min before mixing for another 2.5 min at 285 rpm. Cement paste adhering to the sides of the mixing bowl was scraped and the entire mixture was mixed for another 2.5 min following a 1 min pause. In the test program cement pastes with w/c ratios equal to 0.4, 0.5 and 0.6 were evaluated.

The experimental program comprised of rheological and ultrasonic measurements. Changes in the elastic response and flow behavior of the cement paste sample were evaluated as a function of age using rheological measurements. In addition, changes in the ultrasonic waves, reflected from the hydrating cement paste, were monitored. The evolution of the rheological behavior of cement paste, up to the initiation and early stages of the setting behavior are related to the changes in the microstructure inferred from the ultrasonic measurements. In addition, setting time measurements were also performed using the conventional Vicat needle penetration, to provide a reference. The time zero for all measurements from each procedure corresponds to the time when water was added to the cement powder.

4. Rheological measurements

All rheological measurements were performed using a stress-controlled rheometer with a 14 mm vane tool. A vane tool was chosen for the rheological measurements to minimize the influence of wall slip, which is a problem in high w/c ratio cement pastes [32,33]. The vane tool also offers the advantage that artefacts resulting from large particles are avoided and therefore it has been used for yield stress determination of concentrated suspensions, emulsions and cement paste [34,35]. It has been shown that the storage modulus of cement paste is independent of the measuring tool and the vane tool was shown to produce comparable value of storage modulus when compared to other test geometries such as the parallel plate and the coaxial cylinder.

The diameter and depth of the cup were equal to 28 mm and 60 mm, respectively. The cup was filled with cement paste in three layers. After each layer the cup was vibrated for 10 s. After filling the last layer, the excess cement paste was struck off and the top surface of the cement paste was finished while vibrating. The cup was placed in the rheometer and the vane was inserted to the prescribed depth. Three different measurements were performed for each w/c ratio tested and each test procedure is described in detail below.

4.1. Stress sweep measurements

Stress sweep measurements were performed to determine the yield stress and to establish the linear visco-elastic domain (LVD) of the cement paste. The sample was subjected to an increasing applied stress at a constant rate. It has previously been shown that initially up to a critical value of stress, there is a linear relationship between applied stress and strain. With increasing stress past the critical stress, the response becomes nonlinear eventually producing flow once the yield stress is exceeded. At low applied stress within the LVD, there is little or no change in structure of the material. There is a gradual breakdown of the structure past the LVD. At higher stresses, the structure of the sample is irreversibly destroyed and the material starts to flow as its yield value is exceeded. The material circumscribed by the vane starts moving as a solid cylindrical body [35].

Stress sweep measurements were performed at regular intervals up to 5 h of age or when the capacity of the machine was reached, whichever occurred earlier. Since the structure of the sample is destroyed during the test, each test was performed on a fresh sample. The vane was introduced into the cement paste immediately after placing the sample in the cup, which was then left inside the test machine until the prescribed time.

4.2. Low-amplitude oscillatory shear measurements

The value of applied torque was chosen to be within the linear visco-elastic domain (LVD) of the material. In the test, the vane tool was introduced in the sample immediately after preparing the sample and repeated measurements were made on the same sample.

4.3. Step-stress measurement

A limited number of step-stress measurements were performed on cement paste samples to determine the response of the material to constant applied stress. In this test the cement paste was subjected to stress of a constant magnitude and the resulting strain was monitored. The applied stress was instantaneously increased to the prescribed magnitude and held constant. For each w/c ratio, tests were conducted at two different magnitudes of applied stress, corresponding to values above and below the yield stress of the material. All tests were performed at 1 h after mixing.

5. Oblique ultrasonic measurements

A schematic diagram of the experimental setup for oblique ultrasonic wave reflection measurement is shown in Fig. 1. The experimental system included a function generator, an oscilloscope, a computer and the test probe. The test probe comprises of ultrasonic transducer(s) attached to a buffer plate made of fused quartz, which is in contact with the hardening cement paste. The fused-quartz plate was fabricated with precisely machined, matching, angled faces at angles equal to 0, 30, 40, 50 and 60

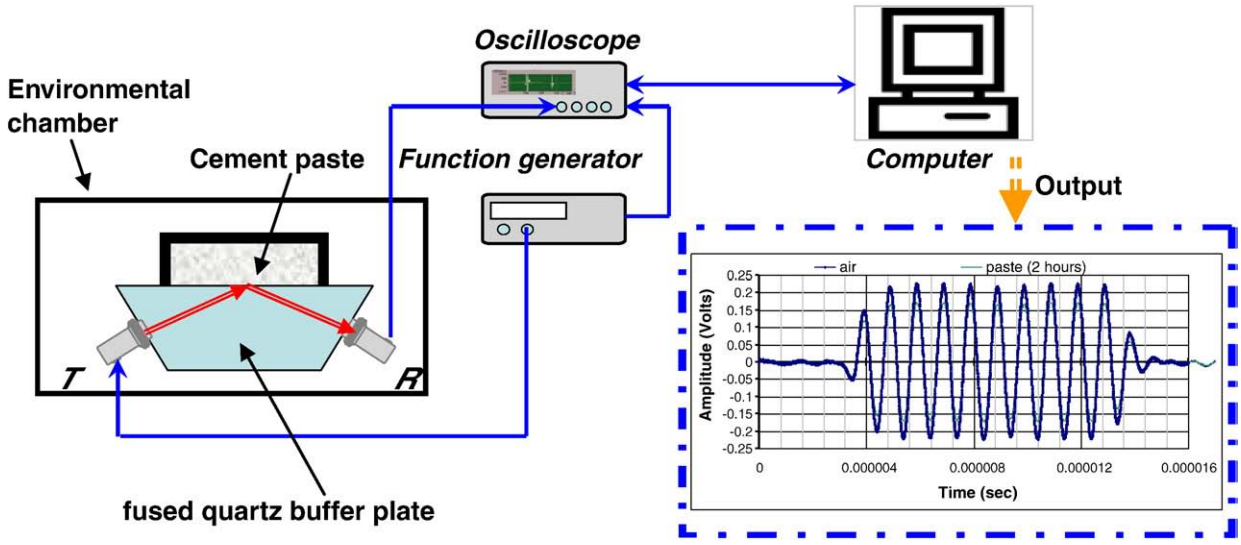

Fig. 1. Schematic diagram of a test setup for ultrasonic measurement.

degrees with respect to the horizontal. Pairs of transducers were mounted on the machined faces at matched angles to collect reflection data at different angles of incidence. The available instrumentation allowed for collecting data from three independent channels. Wave reflection at the fused-quartz/cement paste interface was monitored at 0, 50 and 60 degree angles of incidence. The choice of 50 and 60 degree angles of incidence was based on obtaining the highest sensitivity in measurements. Reflection measurements from sediments have previously shown that highest sensitivity is obtained for incident angles in the range 30 to 70 degrees, and there is a larger change in the amplitude of reflection wave at a larger angle of incidence [36]. The measurements at normal incidence provided a convenient reference for evaluating changes in the reflected waves.

At each angle of incidence, a matched pair of direct contact, ultrasonic shear-wave transducers with a nominal center frequency of 1 MHz, labeled T for transmitting and R for receiving was mounted on the opposite angled surfaces of the buffer plate. The two transducers were aligned precisely at the center of the angled surfaces. While attaching the transducers, the axes of the transducers were aligned to generate a horizontally polarized shear (SH) wave in the fused quartz. A source signal comprising of 1 MHz, 10-cycle, tone burst with pulse repetition period equal to 200 ms was sent by the function generator to the transducer T. Simultaneously, a trigger pulse was sent to the oscilloscope to initialize data capture. The reflected signal detected by transducer R was digitized by the oscilloscope. The data was then transferred to the computer over a GPIB interface for storage and processing. The data acquisition and transfer were controlled by the computer. The oscilloscope had a digitization rate of 500 MS/s which provides a temporal resolution of 2 ns. In each acquisition, 100 waveforms were averaged by the oscilloscope in order to minimize the influence of random noise in the signal. At any given time only one transmitting transducer was active. An averaged waveform was acquired every 30 min allowing sufficient time to take the average and minimize the volume of data collected over a typical monitoring period. The buffer plate and cement paste were placed inside an environmental chamber, which was maintained at 24 °C throughout the duration of the test.

Prior to placing the cement paste sample in the sample holder (attached to the top face of the fused-quartz buffer plate), ultrasonic signals were collected with an empty sample holder. The reflected signals collected from the fused-quartz/air interface were used as reference signals for evaluating the changes in the signal introduced by the cement paste. Immediately after mixing, the cement paste was placed in the sample holder and vibrated for 10 s before initiating data collection. Data processing of the ultrasonic signals comprised of obtaining the amplitude change of the incident wave upon reflection at the fused-quartz/cement paste interface. The change in the amplitude of the wave is given by the amplitude reflection factor, $r(f)$. $r(f)$ was obtained using the self-compensating technique, which involves processing data in the frequency domain [37]. In the frequency domain, the stress wave signals received after a single reflection at the air/quartz and sample/quartz interfaces can be represented as:

$$F^{\text{air/quartz}}(f) = s(f)d_1(f)d_2(f) \tag{5.a}$$

$$F^{\text{sample/quartz}}(f) = s(f)r(f)d_1(f)d_2(f) \tag{5.b}$$

where $F(f)$ is the magnitude of FFT of the captured reflected time domain signal, $d_1(f)$ is the geometric and material signal losses in the couplant, $d_2(f)$ is the material signal losses along the signal path in the elastic fused quartz, $s(f)$ is the input source function, and $r(f)$ is the amplitude reflection coefficient at the bi-material interface. Using the reflected signal from the fused-quartz/air interface as the reference, $r(f)$ at the sample/quartz interface can be determined by normalizing the reflected magnitude off the sample/fused quartz interface with the reflected amplitude off the air/quartz interface [33].

$$r(f) = F^{\text{sample/quartz}}(f) / F^{\text{air/quartz}}(f) \tag{6}$$

The time domain signals were transformed to frequency domain using the FFT algorithm and the amplitude reflection factor at 1 MHz, $r(1)$, was determined as the ratio of the respective magnitudes of the FFT of the ultrasonic signals from the quartz/cement paste and the quartz/air interface at that frequency.

6. Results from rheological measurements

A typical result from an oscillatory stress sweep for cement paste with w/c = 0.4 is shown in Fig. 2. The variation of the elastic component of the shear modulus (G') is plotted as function of the applied shear stress. Nominally similar results were obtained from all w/c ratio tested. From the measured response, a relatively constant value of G' is obtained when the applied shear stress is within the LVD. This is followed by a gradual breakdown of the structure when the magnitude of the applied stress is increased. With increasing stress there, is a decrease in the elastic modulus and eventually, the structure cannot resist the applied stress and it begins to yield. From Fig. 2 changes in the cement paste microstructure produced

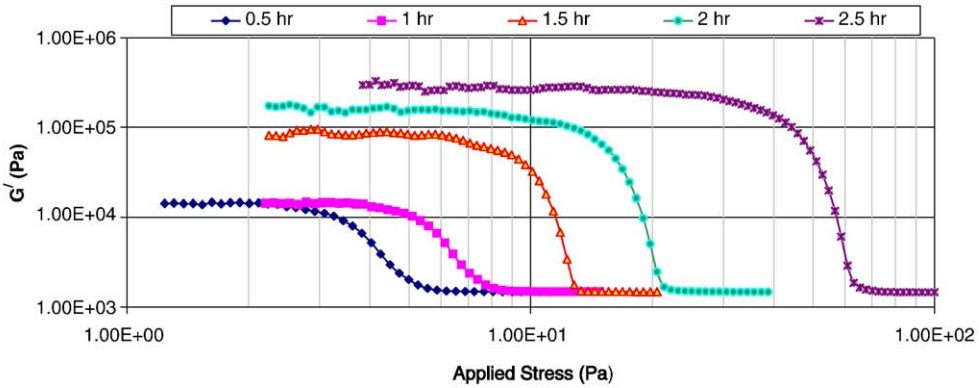

Fig. 2. Results of stress sweep tests on cement paste with w/c = 0.4.

by hydration are evident in the increase in the elastic modulus and yield stress with time.

The increase in the shear modulus obtained from oscillatory shear measurements for cement pastes with the different w/c ratio is shown in Fig. 3(a). The corresponding increase in the yield stress obtained from stress sweep measurements is plotted in the Fig. 3(b) for comparison. The yield stress was determined from the stress sweep measurement of the sample, as the value of the applied stress when the curve starts to deviate more than 10% from the low-stress asymptote [34]. It can be seen that there are similarities between the measured increases in the shear modulus and the yield stress of the material with time. For w/c = 0.5 and 0.6, initially, in the first few hours, there is no significant change in the shear modulus. In this period, there is a very gradual, almost linear increase in the yield stress with time. There is a very rapid, almost exponential increase in both quantities which follows this initial period. In the case of w/c = 0.4, the initial period of inactivity is very short; there is an almost continuous increase in the elastic modulus and yield stress after mixing. In general, cement paste with a lower w/c ratio achieves a fixed value of shear modulus and yield stress earlier in time.

The penetration depths obtained from the Vicat penetration needle test are also shown in Fig. 3(c) to provide a comparison. The time for initial setting determined as per the guidelines of ASTM C-191 [38] for w/c = 0.4, 0.5 and 0.6 are 186, 253 and 327 min, respectively. By comparing the yield stress measurements with the penetration measurements it is immediately obvious that the penetration measurements are not sensitive to the early changes in the microstructure. Changes in the material are more readily evident in the rheological yield stress measurements. While there is an order of magnitude increase in the yield stress, there is no measureable change in the penetration. Discernable changes in the penetration occur significantly later in time than the observed changes in yield stress and shear modulus.

In materials which have a finite yield stress, a stress larger than the yield stress is required to initiate flow [34]. Immediately after mixing, the yield stress of cement paste can be attributed to the resistance offered by the internal structure comprising of agglomerates of cement grains and weak inter-particle forces (if any). When the material goes through setting, there is a decrease in the ability to flow under applied stress. Therefore, the increase in the yield stress is a very good indicator of the setting behavior. Assuming the changes in the arrangements of cement particles (if any) with time are negligible, the increase in yield stress is produced by the products of hydration. It can be reasoned that the sharp rise in the yield stress is associated with the emergence of a continuously connected solid network of cement grains. In a continuously connected network all cement particles are bonded to all the neighboring particles by the products of hydration. Once a continuously

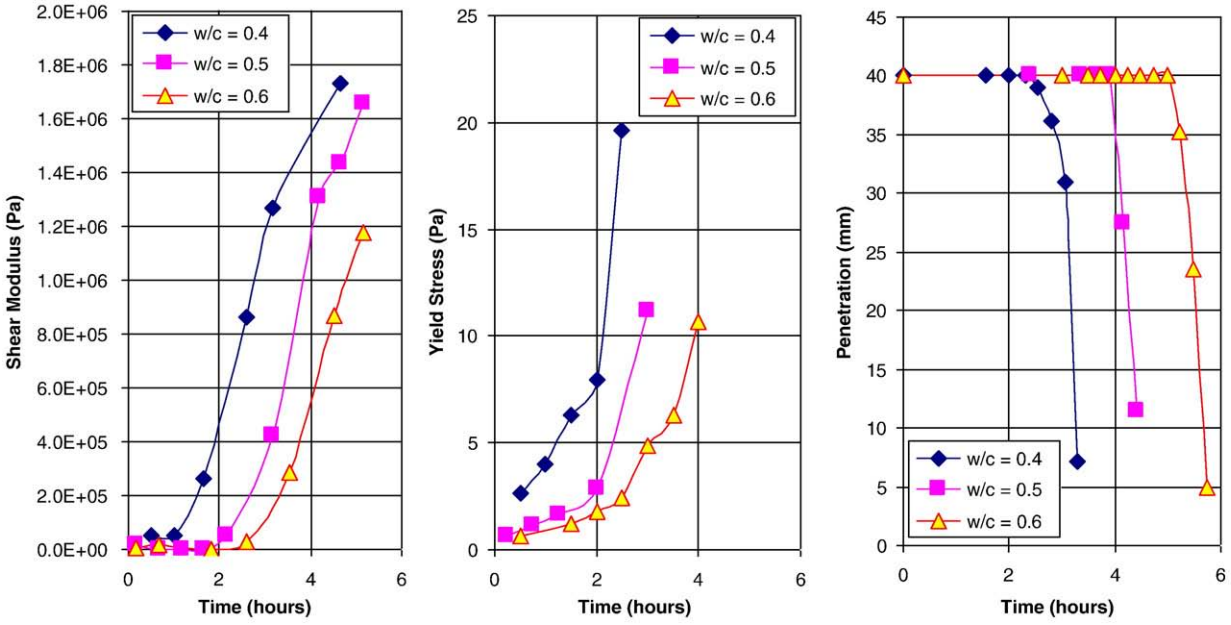

Fig. 3. Increase in shear modulus, yield stress and penetration resistance with time.

connected network of solid grains emerges, small increases in the volume of hydration products within the paste would translate to a significantly higher stress required to produce movement of cement grains relative to the one another. The sharp increase in yield stress can therefore be associated with the initiation of setting behavior within the cement paste. The experimental trends from the rheological measurements suggest that cement pastes with lower w/c set faster than the cement pastes with higher w/c ratio. Measurements indicate that for w/c = 0.5 and 0.6 the yield stress increases after a period when there is a very low rate of change. For w/c = 0.4, however, there appears to be a continuous increase in yield stress after mixing. This suggests that for w/c = 0.5 and higher, a connected network of grains emerges later in time when there is sufficient increase in solid fraction. For w/c = 0.4 on the other hand, the initial state of agglomeration of grains requires a smaller increase in solid fraction to produce a continuously connected solid network.

Typical response from a step-stress measurement for cement paste with w/c = 0.6 is shown in Fig. 4. Nominally similar responses were obtained from all w/c ratio tested. Constant stress measurements were performed at applied torque corresponding to half and 1.2 times the yield stress of the material. At the stress greater than yield stress, the measured rotation appears to reach a steady state, where there is a linear increase in rotation with time. The steady increase in rotation for a constant applied stress is indicative of steady state fluid flow. There is a fundamental difference in the response of cement to constant applied stress of magnitude smaller than the yield stress. The rate of increase in rotation decreases steadily and the rotation approaches an asymptotic value.

The observed rotational response in the step-stress measurement can now be interpreted considering the response of a visco-elastic material subjected constant stress. The steady increase in rotation for a constant applied stress obtained past yield is consistent with the viscous fluid flow under constant stress. In this case, the slope of the constant increase in rotational displacement is related to the viscosity of the liquid. The displacement of the material approaching an asymptotic constant value is consistent with the response obtained from a visco-elastic solid subjected to constant stress.

The results from the response of the material under constant applied stress suggest that even at an early age, before setting, there is a long-range order in the material, which is capable of transmitting low magnitudes of shear stress. While the individual grains of cement may not be bonded to each other, the agglomerates of particles and the inter-particle forces present an internal structure within the material which allows for a buildup of a three-dimensional network of forces to enable the material to resist applied shear. A stable solid-like response is obtained from this network at low deformations. Therefore, for low levels of applied stress, the cement paste can be treated as composed of a solid frame with weakly connected cement grains.

7. Analysis of ultrasonic data

Changes in $r(1)$ and temperature for cement pastes with the different w/c ratios are shown in Fig. 5. The temperature record was obtained from thermocouples placed inside the cement paste and is used as an indicator of the rate of reaction. In all cases, the temperature of the paste initially decreases to 24 °C in the first few hours. The period when there is no perceptible change in the measured temperature may be identified with the dormant period in cement hydration. The increase in temperature after the dormant period signals the beginning of the acceleration stage. Immediately after mixing, the measured $r(1)$ for the three angles of incidence are close to 1.0, suggesting that a significant portion of the incident wave energy is reflected at the quartz–cement paste interface. The general trends in measured changes in $r(1)$ are similar at all incident angles. It can be seen that measurements at a higher angle of incidence give smaller values of $r(1)$ and register larger changes with time. The value of $r(1)$ obtained from normal incident measurement shows the smallest change with time when compared to the corresponding changes from the measurements at oblique incidence. It can be seen that for w/c = 0.4 there is an almost continuous decrease in $r(1)$ after mixing for all angles of incidence. For the case of w/c = 0.6 on the other hand there is no perceivable change in $r(1)$ up to 2 h. There is an increase in the rate of change of $r(1)$ with time. Starting from a gradual rate of change there is an accelerated change at later times. It can also be seen that while the measured response from all w/c ratios are nominally similar, there is larger decrease in $r(1)$ with time for smaller w/c ratio. It is interesting to note that there is a marked decrease in $r(1)$ before the end of the dormant period indicated by the temperature measurements. It should be mentioned that the accuracy in temperature measurements was on the order of ± 0.5 °C which may not be sufficient for discerning small temperature changes in this period.

The measured changes in the $r(1)$ at the fused-quartz/cement paste interface can now be interpreted in terms of the expected result from the reflection of an SH wave at the interface between an elastic and a

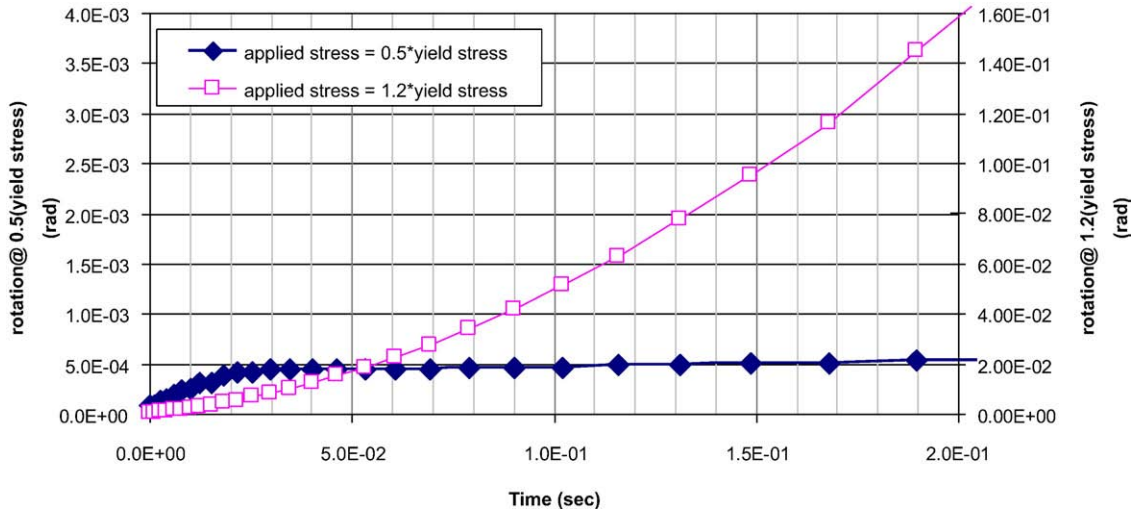

Fig. 4. Step-stress response of cement paste with w/c = 0.6 at two different magnitudes of applied stress.

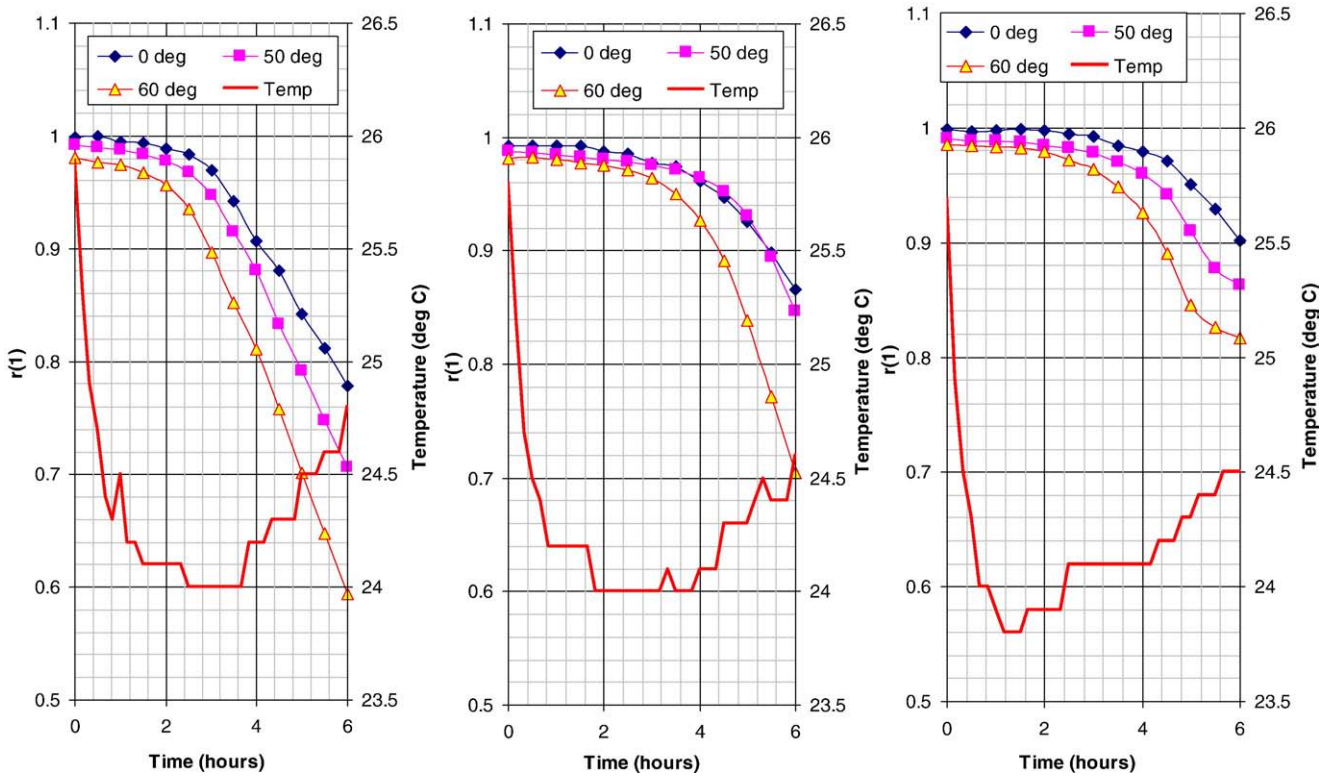

Fig. 5. Amplitude reflection factor, r(1), at different angles of incidence for w/c = 0.4, w/c = 0.5 and w/c = 0.6.

poroelastic material (Fig. 6). In the poroelastic idealization, the hydrating cement paste is assumed to be comprised of a water-filled porous skeleton. The material of the skeleton is assumed to be homogenous and isotropic. Reflection of a planar wave, initially traveling in an elastic medium, incident on an interface with poroelastic material would produce changes in both amplitude and phase of the wave. For a poroelastic material with known properties (internal system variables are known), the exact magnitude of $r(f)$ after reflection can be obtained considering dynamic equilibrium and displacement continuity at the interface [18]. The conditions for dynamic equilibrium and the form of the expressions for $r(f)$ are summarized in Appendix A.

For an SH wave traveling in an elastic material, incident at the interface with the poroelastic material, changes in the amplitude and phase of the wave following reflection from the poroelastic material can be symbolically expressed as

$$R_s = r(f)e^{i\Phi} = R_s(\rho_e, E_e, \nu_e, \rho_s, \rho_f, K_f, \mu_b \beta, \eta, \alpha, c, \kappa, \delta_\mu) \quad (7)$$

where ρ_e, E_e, and ν_e are the density, the Young's modulus and the Poisson's ratio of the fused quartz. μ_b is the shear modulus of the skeletal frame (under drained conditions) which is a real value to present the properties under the static conditions. For the porous medium, the dynamic shear modulus of the skeletal frame is given by a complex number

$$\overline{\mu}_b = \mu_b(1 + \delta_\mu i)$$

where the loss factor δ_μ, was introduced by Stoll to consider the energy loss due to the friction among the phases of porous media. δ_μ is usually a small number in the range of 0.11–0.17 [18,39]. The information about the poroelastic material is contained in the reflection coefficient $r(f)$. Considering the relationships between tortuosity, permeability, pore size and porosity, in Eqs. (3) and (4), the number of independent variables in the expression of R_s can be decreased

$$R_s = R_s(\rho_e, E_e, \nu_e, \rho_s, \rho_f, K_f, \mu_b, \beta, \eta, \delta_\mu) \quad (8)$$

Determination of R_s as described by Eq. (8), requires the input of several internal system variables of the porous medium. When applied to the case of hydrating cement paste, some simplifications can be introduced to the expression for R_s, assuming the hydrating cement paste is a water-filled porous skeleton made up of cement grains and products of hydration. The bulk properties of water are readily available as $K_f = 2.2 \times 10^9$ Pa, and the viscosity $\eta = 0.9 \times 10^{-3}$ kg/ms. Further, changes in density of the hydrating cement paste with age (on account of chemical shrinkage) can be considered to produce insignificant changes in the bulk density of the material. Thus considering the

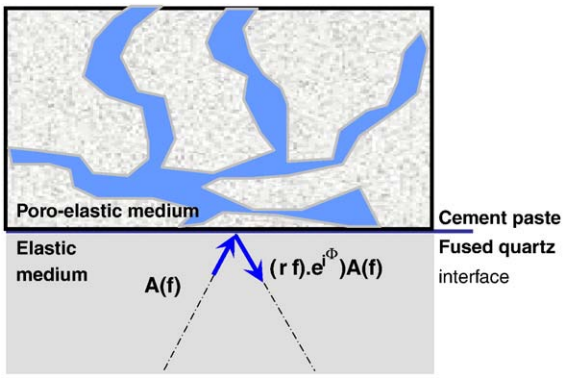

Fig. 6. Schematic representation of ultrasonic wave reflection at the interface between elastic and poroelastic materials.

hydrating cement material to be composed of two components, the porous skeleton and water, a simple relation can be obtained considering composite theory

$$\rho_{bulk} = (1-\beta)\rho_s + \beta\rho_f \tag{9}$$

where, ρ_{bulk} is the density of the cement paste. ρ_{bulk} can be considered to be constant through the hydration process. The ρ_{bulk} of cement paste samples with w/c = 0.4, 0.5 and 0.6 were determined at three days of age and were found to be 1.98, 1.87 and 1.77 g/cm^3, respectively. Using this value, the ρ_s, which represents the effective density of the solid material, can be obtained using Eq. (9), further reducing the number of internal variables in the expressions for R_s.

$$R_s = R_s(\rho_e, E_e, \nu_e, \mu_b, \beta, \delta_\mu) \tag{10}$$

Since the material properties of fused quarts are readily available, the reflection at the fused-quartz/cement paste interface can be expressed in terms of the two key internal system variables, porosity and shear modulus of the skeleton, as

$$R_s = R_s(\mu_b, \beta, \delta_\mu). \tag{11}$$

These internal system variables which describe the poroelastic material are functions of age (time after mixing). Since the obtaining analytical expressions for the inversion of the internal variables form the expression for R_s is intractable, numerical inversion was performed to optimize the material constants such that the theoretical prediction is close to the experimental response. The experimental data used in the optimization comprised of the $r(1)$ at three different angles of incidence. The Generalized Reduced Gradient nonlinear optimization scheme was used to minimize an objective function given as

$$F(c_i) = \sqrt{\frac{\sum_{n=1}^{3} \left(|R_s^{exp}(\theta_n, c_i)| - |R_s^{theo}(\theta_n, c_i)|\right)^2 / |R_s^{exp}(\theta_n, c_i)|}{3}} \tag{12}$$

where θ_n is the discrete incident angle at which experimental values are obtained, and c_i are the internal system variables of the poroelastic solid. For the numerical inversion, the starting guess of porosity for the first measurement after mixing was obtained using the relation

$$\beta = \frac{\rho_{cem}(w/c)}{1 + \rho_{cem}(w/c)} \tag{13}$$

where ρ_{cem}, the specific gravity of cement was assumed to be 3.2. The starting guess for μ_b was taken as 10^5 Pa. The range for δ_μ was initially prescribed to be within 0.01–0.3. It was found that within the prescribed range, there was no influence of δ_μ on the final values of μ_b and β. The solution obtained at a given time was then used as the starting guess for the next time.

The shear modulus and porosity of the cement paste obtained from the numerical inversion of the test data are shown in Fig. 7. The initial values of shear modulus and porosity obtained immediately after mixing were (8.56×10^5 Pa, 0.555), (3.59×10^5 Pa, 0.611) and (1.58×10^5 Pa, 0.653) for cement pastes with w/c = 0.4, 0.5 and 0.6, respectively. The trends in the shear modulus increase obtained from the ultrasonic measurements are qualitatively similar to those obtained from the oscillatory shear rheological measurements. There appears to be an exponential increase in shear modulus following a period when there is no noticeable change. Consistent with established results a higher rate of modulus increase is obtained for a lower w/c ratio. Cement paste with w/c = 0.4 exhibits the most rapid increase in modulus, while cement paste with w/c = 0.6 exhibits an extended period when there is no noticeable change followed by a slower rate of increase. The rate porosity change are also significantly higher for cement paste with w/c = 0.4 when compared to the other two w/c ratios. In the cement paste with w/c = 0.4 there appears to be an almost continuous change in porosity after mixing. Cement paste with w/c = 0.6, on the other hand, exhibits an insignificant change in porosity up to 4 h, following which there is a rapid decrease.

The porosity obtained from the ultrasonic data corresponds to relative proportion of the water-filled space within a solid skeleton. The measured decrease in porosity is therefore equal to the increase in the solid fraction within the cement paste. The increases in the solid fraction with time are shown in Fig. 8. It can be seen that for w/c = 0.4, there is an almost continuous increase in the solid fraction with time. Cement paste with w/c = 0.6 on the other hand exhibits a prolonged period with relatively little change in the microstructure. After 2 h, both w/c = 0.4 and 0.5 exhibit an almost linear increase in solid fraction with time. It is interesting to note that while the increase in the solid fraction for both w/c = 0.4 and 0.5 is linear with time, correspondingly, there is an exponential change in the elastic modulus. Comparing the relative changes in the shear modulus and

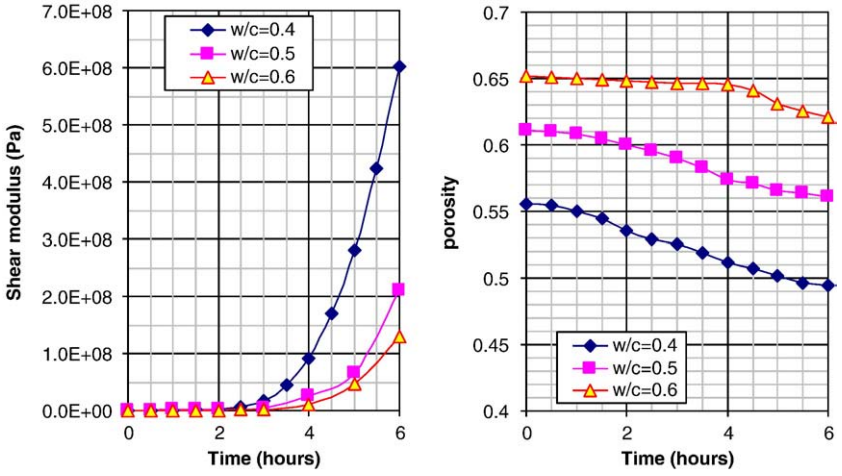

Fig. 7. Shear modulus and porosity of cement paste obtained from inversion of ultrasonic data.

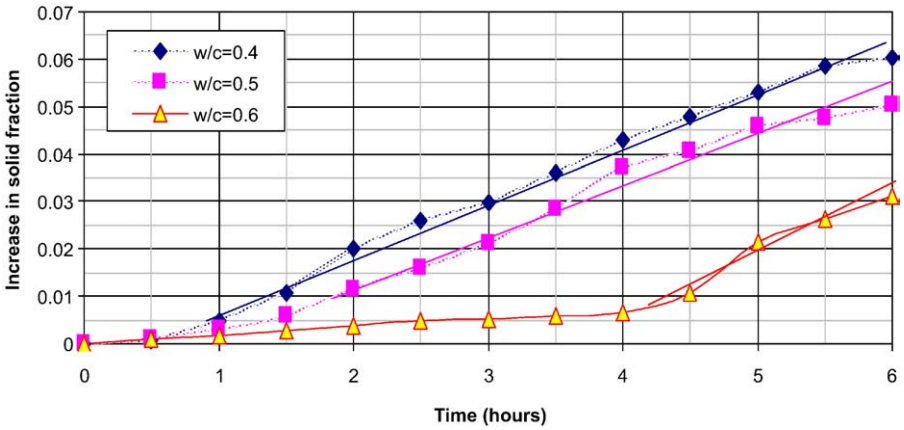

Fig. 8. Increase in solid fraction within the cement paste as a function of time.

porosity obtained from the ultrasonic data, it is interesting to note that there is a three order of magnitude increase in the shear modulus corresponding to relatively small change in the porosity. There is hence a very non-linear relationship between the decrease in porosity and increase in modulus. After 2 h, the rates of increase in the solid fraction for w/c = 0.4 and 0.5 are comparable. w/c = 0.4, however, exhibits a significantly higher rate of increase of elastic modulus. This suggests that for a lower w/c ratio, because of the initial closer spacing of cement grains a smaller volume of hydration products produce a higher change in the shear modulus.

8. Discussion

In the previous sections, the development of microstructure was evaluated in terms of internal system variables of a poroelastic material, which provides identical acoustic properties as the hydrating cement paste. The application of the poroelastic idealization for interpreting response of the material to the low-amplitude shear stress produced by an ultrasonic wave is supported by the evidence of the solid-like response obtained in the step-stress rheological measurements. Ultrasonic waves used in this study assess changes in the microstructure at a length scale corresponding to the wavelength. Considering the range of shear moduli and densities of cement paste with the different w/c ratios, the wavelength within the period of observation ranges from 10^{-5} m, initially, to 10^{-4} m at 6 h. Ultrasonic measurements therefore provide indication of changes at these small length scales. The increase in the solid fraction indicates that there is an almost continuous change in microstructure after mixing at this small length scale.

A comparison between the shear moduli obtained from the rheological and ultrasonic measurements is shown in Fig. 9. The shear modulus obtained from the ultrasonic measurements is a few orders of magnitude higher than the corresponding value from rheological measurement. This is consistent with established findings in materials which exhibit frequency dependent moduli, where the dynamic properties determined at higher frequencies are higher than those obtained at lower frequencies. It should also be noted that the shear modulus obtained from the rheological measurements relates to the bulk of the material while the ultrasonic measurements provide a measure of the stiffness of the solid skeleton. The results from the different w/c ratios however suggest that there is unique relationship between the low and high frequency shear moduli.

The results from the two measurement techniques can now be compiled to develop an understanding of the changes in the microstructure which produce setting in cement pastes. The increase in the shear modulus of the solid obtained from the ultrasonic measurements is compared with the increase in yield stress from rheological measurements in Fig. 10. It can be seen that there is a high level of correspondence between the two quantities. The sharp rise in the yield, which signals the emergence of a fully connected solid network within the cement paste, coincides in time with the observed sharp increase in shear modulus with time. The high level of correspondence between the two measurements suggests that the emergence of a continuously connected solid coincides with significant increases in the shear modulus of the skeleton. Therefore, if yield stress is taken as an indicator of setting in cement paste, the rapid increase in the rapid rise in shear modulus obtained from ultrasonic measurements can be used to determine the point in time when a continuously connected solid emerges within the cement paste.

Relating the changes in the shear modulus and yield stress obtained from rheological measurements with the changes in porosity from the ultrasonic data, it can be seen that there is a larger change in elastic modulus than yield stress for a given decrease in porosity. Changes in porosity are produced when the water is replaced with products of hydration. The formation of hydration products produces a larger relative increase in elastic modulus than yield stress. Measurements for elastic modulus are associated with infinitesimal relative motions between the individual grains and do not disturb the arrangement of

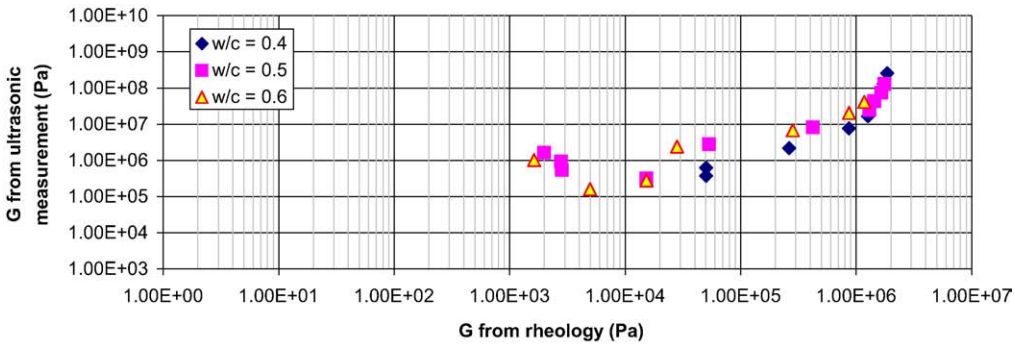

Fig. 9. Comparison between shear moduli from rheological and ultrasonic measurements.

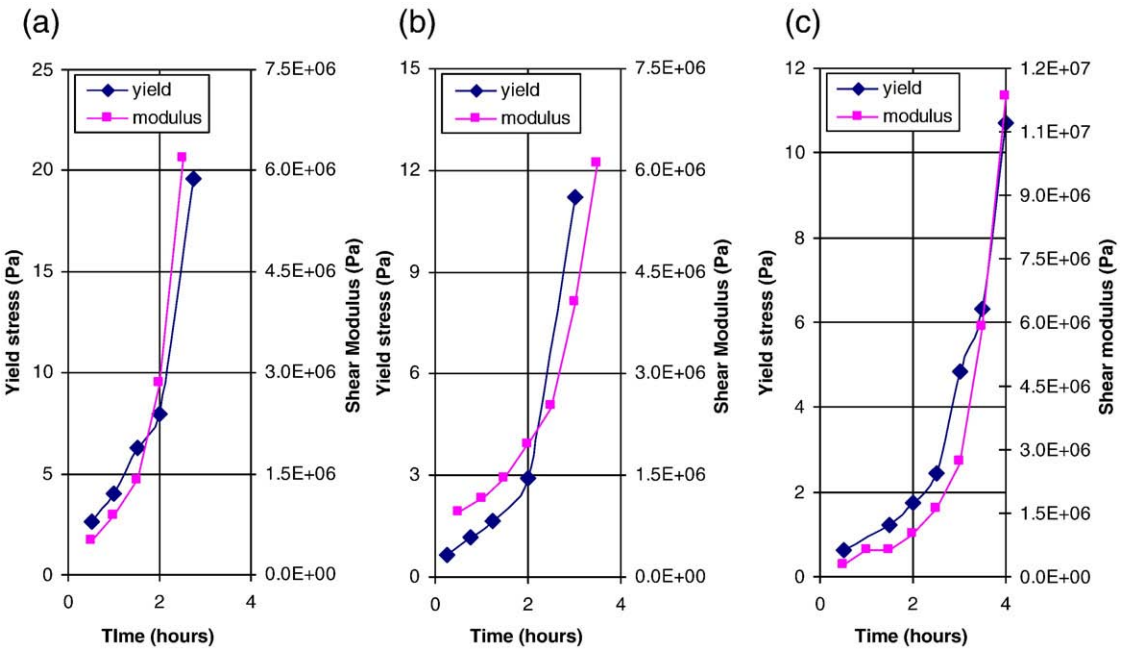

Fig. 10. Comparison between the yield stress and shear modulus increases for different w/c ratios: (a) w/c = 0.4; (b) w/c = 0.5; and (c) w/c = 0.6.

grains. Yield stress, the stress required to initiate flow, on the other hand, depends upon the effort for individual grains to move relative to the other grains and on the capacity of the bond between the individual grains. Yield stress is therefore related to the stress required to produce large relative movements between the grains. In the early stages of hydration, the formation of the hydration products and their placement contribute to a larger relative increase in inter-particle elastic interaction between cement grains than the force required to produce a large separation between the grains.

The technique presented here has been shown to be very sensitive to changes in the internal structure, influenced by the buildup of solidity, which brings about setting in cement pastes. In ultrasonic measurements, heterogeneous media appear homogeneous when waves have a wavelength, which is large compared to the scale of heterogeneity. The resolution of length scale from an ultrasonic measurement therefore corresponds with the wavelength of the wave. Considering the frequency of 1 MHz, the wavelength of the wave in the material varies from 10^{-6} to 10^{-5}m during setting, which provides a reasonable overlap with the dimensions of pore network comprised of the continuous water-filled space in a packing of cement grains.

In measurements which are based on reflection at the surface of the material there are always issues related to penetration of waves and the interface where the material properties are different than the interior of the material. The long-range order of microstructure is disrupted at the interface or boundary when compared with the bulk material. Acoustic impedance determination from ultrasonic measurements on mortar and concrete specimens has shown that this effect persists for a few millimeters from an interface or boundary [40]. The length scale of the interface was found to correspond with the maximum size of the heterogeneity (aggregate). For measurements in this study, the size of the interface would confirm to the cement grain size, which corresponds well with the wavelength. Therefore, the influence of the interface would be less critical in measurements involving cement paste. Despite the larger size of interface region, the technique presented here can potentially be extended to investigating the setting behavior in concrete. It has been shown that the relative changes in the acoustic impedance at the interface obtained from reflection measurements were identical to the corresponding evolution in the acoustic impedance in the bulk material since both are controlled by hydration [40]. This is further supported by previous measurements on slabs, where ultrasonic shear reflection measurements at normal incidence have been shown to correlate well with strength gain in concrete [13]. Reflection measurements from mortar have also been shown to correlate well with setting time determined using pin penetration [14]. The ultrasonic measurements presented here also correlate well with the rheological response, which is a measure of bulk behavior.

9. Conclusions

Combining the information obtained from ultrasonic and rheological measurements allows for relating changes in the microstructure with the mechanical properties of hydrating cement paste through setting. Specifically,

1. Low-amplitude stress measurements indicate that even for a high w/c ratio, there is sufficient long-range order within the material to resist the applied shear stress.
2. After mixing, there is a continuous evolution of microstructure at the length scales corresponding to the wavelength of the ultrasonic wave. For all w/c ratios tested, there is a continuous increase in the solid fraction associated with the products of hydration after mixing. There is a slower rate of increase in the solid fraction for a higher w/c ratio.
3. A decrease in porosity (an increase in solidity) produced by the products of hydration results in an increase in shear modulus and yield stress. There is a larger relative increase in modulus than yield stress for a given decrease in porosity.
4. Penetration measurements do not provide sufficient sensitivity to detect the early changes in the microstructure.
5. Both rheological and ultrasonic measurements indicate changes in the material behavior which are not detected by the penetration measurements. Setting behavior indicated by a sharp rise in the yield stress occurs at a time when the penetration measurements indicate no change in the material response.
6. Setting behavior within cement paste, associated with a sharp increase in the yield stress of the material is indicative of the formation of a continuously connected solid network.

7. The sharp increase in the yield stress is coincident with a sharp increase in the shear modulus of the solid obtained from the ultrasonic measurements.

Acknowledgements

The authors would like to acknowledge the help and guidance provided by Prof. Morton Denn, in interpreting the rheology data. Financial support from NSF (CMS grant CAREER CMS 0238692) is also gratefully acknowledged.

Appendix A

Wave propagation in a poroelastic medium

To solve the Equation(s) 1, it is convenient to express the displacement vectors in terms of scalar and vector potentials

$$\vec{u} = \nabla\phi_s + \nabla \times \vec{\varphi}_s \text{ and } \vec{w} = \nabla\phi_f + \nabla \times \vec{\varphi}_f. \quad \text{(A1.a and b)}$$

By substituting Equation(s) A1 in Equation(s) 1, two pair of equations are obtained in terms of potentials

$$\begin{cases} H\nabla^2\phi_s - C\nabla^2\phi_f = \rho\ddot{\phi}_s - \rho_f\ddot{\phi}_f \\ C\nabla^2\phi_s - M\nabla^2\phi_f = \rho_f\ddot{\phi}_s - m'\ddot{\phi}_f - (\eta/k)\dot{\phi}_f \end{cases} \quad \text{(A2)}$$

and

$$\begin{cases} \mu_b\nabla^2\vec{\varphi}_s = \rho\ddot{\vec{\varphi}}_s - \rho_f\ddot{\vec{\varphi}}_f \\ (\eta/k)\vec{\varphi}_f = \rho_f\ddot{\vec{\varphi}}_s - m'\ddot{\vec{\varphi}}_f \end{cases}. \quad \text{(A3)}$$

Both Eqs. (A2) and (A3) admit harmonic solutions. Eq. (A2) governs the compression wave propagation, while the Eq. (A3) determines the shear waves propagation. The solutions for the shear wave could be written as

$$\begin{cases} \vec{\varphi}_s = \boldsymbol{C}\exp[j(\omega t - \vec{k}\cdot\vec{r})] \\ \vec{\varphi}_f = \boldsymbol{D}\exp[j(\omega t - \vec{k}\cdot\vec{r})] \end{cases} \quad \text{(A4)}$$

where $\vec{k}$ is a complex vector (complex wave number), $\vec{r}$ is the position vector and ω is the frequency of waves. The real part of $\vec{k}$ determines the direction of the normal to planes of equal phase, the imaginary part determines the directions of the normal to planes of equal amplitudes. When Eq. (A4) are substituted into Eq. (A3), equations for obtaining the wave number are obtained

$$(\rho\omega^2 - \bar{\mu}_b {k_{sh}}^{*2})(m'\omega^2 - i\omega F(\omega)\eta/k_0) - (\rho_f\omega^2)^2 = 0 \quad \text{(A5)}$$

where $F(\omega)$, is a frequency correction function for the viscosity η, introduced by Biot, to represent that the friction force of fluid resulting from out-of-phase rate of flow relative to the solid. $F(\omega)$ was derived as a complex quantity by Biot, considering three-dimensional flow in a circular duct and is given as

$$F(\chi) = \frac{1}{4}\frac{\chi T(\chi)}{1 - 2T(\chi)/j\chi} \quad \text{(A6a)}$$

where

$$T(\chi) = \frac{ber'(\chi) + jbei'(\chi)}{ber(\chi) + jbei(\chi)}, \quad \text{(A6b)}$$

$$\chi = (\omega\alpha^2/\eta)^{1/2} \quad \text{(A6c)}$$

The functions $ber(\chi)$ and $bei(\chi)$ are the real and imaginary parts of the Kelvin function. The factor α represents the pore size. The shear wave number can be obtained from Eq. (A5) in the following form

$${k_{sh}}^{*2} = [\rho\omega^2 - \frac{(\rho_f\omega^2)^2}{m'\omega^2 - j\omega(F\eta/k_0)}]/\bar{\mu}_b. \quad \text{(A7)}$$

Oblique SH wave reflection

SH wave incidence at an interface between an elastic and a poroelastic material is considered. Assuming an SH wave traveling in an elastic material is incident at an angle θ at the interface, shown in Fig. 11, the potentials of incident, reflected and refracted waves are given as

$$\varphi_i(x,z) = A_i\exp[j(\omega t - k_1\cos(\theta)z - k_c x)] \quad \text{(A8)}$$

$$\varphi_r(x,z) = A_r\exp[j(\omega t + k_1\cos(\theta)z - k_c x)] \quad \text{(A9)}$$

$$\varphi_{ts}(x,z) = A_{ts}\exp[j(\omega t - k^*_{sh}\cos(\alpha)^* z - k_c x)] \quad \text{(A10)}$$

$$\varphi_{tf}(x,z) = A_{tf}\exp[j(\omega t - k^*_{sh}\cos(\alpha)^* z - k_c x)]. \quad \text{(A11)}$$

In developing the equations for the potentials, Snell's law has been implicitly applied such that all the potentials which are generated at the interface give the same projection of the propagation vector on the interface.

$$k^*_{sh}\sin(\alpha)^* = k_1\sin(\theta) = k_c \quad \text{(A12)}$$

The boundary conditions at the interface, $z=0$, are given as

(1) For the continuity of displacement

$$u_y|_{elastic} = u_y|_{porous} \text{ or } \frac{\partial\varphi_i}{\partial z} + \frac{\partial\varphi_r}{\partial z} = \frac{\partial\varphi_{ts}}{\partial z} \quad \text{(A13)}$$

(2) For the equilibrium of tangential stress.

$$\tau_{yz}|_{elastic} = \tau_{yz}|_{porous} \text{ or } \mu_1(\frac{\partial^2\varphi_i}{\partial z^2} + \frac{\partial^2\varphi_r}{\partial z^2}) = \bar{\mu}_b\frac{\partial^2\varphi_{ts}}{\partial z^2} \quad \text{(A14)}$$

(3) Continuity of fluid movement. It has the same boundary conditions with the previous case, and this conditions is satisfied automatically because of the characteristics of the SH wave mode.

The ratios of the amplitudes of the potentials can be obtained as

$$\frac{A_r}{A_i} = \frac{\bar{\mu}_b k^*_{sh}\cos(\alpha)^* - \mu_1 k_1\cos(\theta)}{\bar{\mu}_b k^*_{sh}\cos(\alpha)^* + \mu_1 k_1\cos(\theta)}, \quad \text{(A15)}$$

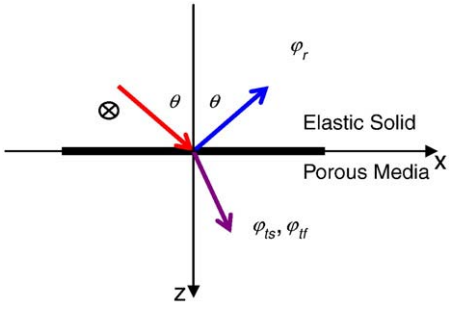

Fig. 11. Reflection and refraction at the interface with oblique SH incidence.

$$\frac{A_{ts}}{A_i} = \left(\frac{2\mu_1 k_1 \cos(\theta)}{\overline{\mu}_b k_{sh}^* \cos(\alpha)^* + \mu_1 k_1 \cos(\theta)}\right) \frac{k_1 \cos(\theta)}{k_{sh}^* \cos(\alpha)^*} \quad \text{(A16)}$$

$$\frac{A_{tf}}{A_i} = \left(\frac{2\mu_1 k_1 \cos(\theta)}{\overline{\mu}_b k_{sh}^* \cos(\alpha)^* + \mu_1 k_1 \cos(\theta)}\right) / \left(\frac{k_{sh}^* \cos(\alpha)^*}{k_1 \cos(\theta)} \frac{\rho_f \omega^2}{\rho\omega^2 - \overline{\mu}_b (k_{sh}^*)^2}\right). \quad \text{(A17)}$$

References

[1] J.J. Thomas, H.M. Jennings, A.J. Allen, Concrete Science and Engineering 1 (1999) 45–64.
[2] M.C.G. Juenger, V.H.R. Lamour, P.J.M. Monteiro, E.M. Gartner, G.P. Denbeaux, Journal of Materials Science Letters 22 (2003) 1335–1337.
[3] T.J. Chotard, M.P. Boncoeur-Martel, A. Smith, J.P. Dupuyb, C. Gaulta, Cement and Concrete Composites 25 (1) (2003) 145–152.
[4] J.J. Thomas, H.M. Jennings, J.S. Gevrenov, G. Constantinides, F.-J. Ulm, Cement and Concrete Research 37 (2007) 329–336.
[5] D.P. Bentz, E.J. Garboczi, C.J. Haeckerb, O.M. Jensen, Cement and Concrete Research 29 (10) (1999) 1663–1671.
[6] G. Ye, K. van Breugel, et al., Cement and Concrete Research 33 (2) (2003) 233–239.
[7] J. Keating, D.J. Hannant, A.P. Hibbert, Cement and Concrete Research 19 (1989) 554–566.
[8] R. D'Angelo, T. Plona, L. Schwartz, P. Coveney, Advanced Cement Based Materials 2 (1) (1995) 8–14.
[9] Z. Sun, T. Voigt, S.P. Shah, Cement and Concrete Research 36 (2006) 278–287.
[10] C.U. Grosse, S.U. Koble, H.W. Reinhardt, Ultrasound, Scanning Electron Microscopy and Nuclear Magnetic Resonance Spectroscopy — Comparison of Results Investigating the Hydration Process in Cementitious Materials, vol. 6 No. 5, 2001, NDT.net - May 2001.
[11] RILEM TC-185-ATC, in: H.W. Reinhardt, C.U. Grosse (Eds.), Advanced Testing of Cement-Based Materials during Setting and Hardening — Final Report of RILEM TC 185-ATC, RILEM, Bagneux, France, 2005.
[12] K.V. Subramaniam, J. Lee, Ultrasonic Assessment of Early-age Changes in the Material Properties of Cementitious Materials, Materials and Structures, vol. 40, No. 3, RILEM, 2007, pp. 301–309.
[13] K.V. Subramaniam, J.P. Mohsen, C. Shaw, S.P. Shah, ACI Materials Journal 99 (5) (2002) 458–462.
[14] K.V. Subramaniam, J. Lee, B. Christensen, Cement and Concrete Research 35 (5) (2005) 850–857.
[15] T. Voigt, Y. Akkaya, K.V. Subramaniam, S.P. Shah, Journal of Materials in Civil Engineering 15 (3) (2003) 247–254.
[16] D. Johnson, T. Plona, Journal of the Acoustical Society of America 72 (1982) 556.
[17] D. Johnson, P. Sen, Physical Review B 24 (5) (1981) 2486–2496.
[18] R. Stoll, T. Kan, Journal of the Acoustical Society of America 70 (1981) 149.
[19] N.P. Chotiros, Journal of the Acoustical Society of America 94 (1995) 199–214.
[20] T. Yamamoto, A. Turgut, Journal of the Acoustical Society of America 83 (1988) 1744–1751.
[21] T. Bourby, O. Cousy, B. Zinszer, Acoustics of Porous Media, Gulf Publishing Company, Houston, TX, 1987.
[22] H.F.W. Taylor, "Portland Cement: Hydration Products," a publication of Materials Education Council, Materials Research Laboratory, University Park, PA, 1985.
[23] P.L. Pratt, H.M. Jennings, Annual Review of Materials Science 11 (1981) 123–149.
[24] M. Biot, Journal of the Acoustical Society of America 28 (1956) 168.
[25] M. Biot, Journal of the Acoustical Society of America 28 (1956) 179.
[26] M. Biot, Journal of Applied Physics 33 (1962) 1482.
[27] C. Zimmerman, M. Stern, Journal of Engineering Mechanics, ASCE 120 (1994) 2154.
[28] J. Berryman, Applied Physics Letters 37 (1980) 382.
[29] T. Plona, Applied Physics Letters 36 (1980) 259.
[30] D. Williams, A. Saak, H.M. Jennings, Cement and Concrete Research 29 (9) (1999) 1491–1496.
[31] ASTM C 305, Annual book of ASTM Standards, American Society for Testing Materials, West Conshohocken, PA, 2001.
[32] L. Nachbaur, J.C. Mutin, A. Nonat, L. Choplin, Cement and Concrete Research 31 (2) (2001) 183–192.
[33] A.W. Saak, H.M. Jennings, S.P. Shah, Cement and Concrete Research 31 (2) (2001) 205–212.
[34] T. Mezger, The Rheology Handbook: For Users of Rotational and Oscillatory Rheometers, Vincent Verlag, Hannover, Germany, 2006.
[35] A.W. Saak (1999)" Characterization and Modeling of the Rheology of Cement Paste: With Applications Towards Self-Flowing Materials, PhD thesis, Northwestern University, Evanston, IL.
[36] M.J Isakson, T. Neilsen, A. Worley, in: A. Caiti, N.R. Chapman, J.-P. Hermand, S.M. Jesus (Eds.), Inversions of Reflection Loss Measurements of a Smotth Water/Sand Interface, Acoustic Sensing Techniques for the ShallowWater Environment, Springer Verlag, Netherlands, 2006, pp. 213–231.
[37] J.D. Achenbach, I.N. Komsky, Y.C. Lee, Y.C. Angel, Journal of Nondestructive Evaluation 11 (2) (1992) 103–108.
[38] ASTM C 191, Annual book of ASTM Standards, American Society for Testing Materials, West Conshohocken, PA, 2001.
[39] N.P. Chotiros, Journal of the Acoustical Society of America 112 (5) (2002) 1853–1868.
[40] T. Ozturk, O. Kroggel, and P. Grubl, "Validity of the common direct correlation between reflection data and volume characteristics of concrete," in Advanced Testing of Fresh Cementitious Materials, pp. 95–109, August 3–4, Stuttgart, Germany (ISBN 3-980 8542-6-4), 2006.